JOURNAL OF PROPULSION AND POWER
Vol. 16, No. 4, July–August 2000

Effect of Initial Velocity Profile on the Development of Round Jets

E. Ferdman,* M. V. Ötügen,† and S. Kim‡
Polytechnic University, Brooklyn, New York 11201

The effects of nonuniform initial velocity profiles on the downstream evolution of round turbulent incompressible jets have been investigated experimentally. Jets evolving from two nonuniform initial velocity profiles, one with an axisymmetric fully developed profile and the other with an asymmetric initial profile, were compared to jets with top-hat initial velocity distributions. The Reynolds number of the present jets was 2.4×10^4, based on the exit bulk velocity and the source diameter. The jets exited from pipes of circular cross section. For the jet with the axisymmetric initial velocity, the pipe was straight and produced a fully developed profile at the exit. For the jet with the initially asymmetric velocity distribution, the flow passed through a 90-deg bend in the pipe before exiting. Velocity measurements were carried out using hot-wire anemometry extending from the exit plane up to 80 jet diameters downstream. The evolution of both jets towards a self-preserving state is rapid. The initial asymmetry of the second jet vanishes by 9 pipe diameters. By 15 pipe diameters, the mean velocity profiles of both jets are self-preserving and follow very well the Gaussian distribution. Although the far-field mean and turbulent trends of the present jets are qualitatively similar to those jets with uniform initial-velocity distributions, there are some quantitative differences between them. The present jets develop into a self-preserving state faster than those jets with a uniform initial-velocity profile. On the other hand, the initial growth of turbulence intensities and the far-field decay rates of the present jets are smaller than the jets with uniform initial-velocity profiles.

Nomenclature

A	= cross-sectional area
a, a_e	= constants defining the velocity decay rate
b_u	= jet velocity half-width
D	= pipe diameter
D_E	= jet effective diameter
De	= Dean number, $(D/2R)^{0.5}Re$
d, d_e	= constants defining the jet growth rate
$\dot{F}$	= specific momentum flux
L	= longitudinal integral length scale
$\dot{M}$	= mass flux
R	= radius of curvature of pipe bend
Re	= Reynolds number, $\rho U_b D/\mu$
U	= mean axial velocity
U_b	= exit bulk velocity based on mass flux
$U_{b,1}$	= exit bulk velocity based on momentum flux
u'	= rms of fluctuating axial velocity
$u'v'$	= Reynolds shear stress
v'	= rms of fluctuating lateral velocity
x	= axial coordinate measured from pipe exit
y	= lateral coordinate on jet symmetry plane
z	= coordinate normal to the jet symmetry plane
μ	= kinematic viscosity
μ_t	= turbulent viscosity
ρ	= density of air

Subscripts

cl	= jet centerline
e	= jet exit
m	= local maximum

Received 14 July 1998; presented as Paper 99-0159 at the AIAA 37th Aerospace Sciences Meeting, Reno, NV, 11–14 January 1999; revision received 22 April 1999; accepted for publication 15 June 1999.

*Graduate Assistant, Mechanical, Aerospace, and Manufacturing Engineering Department, Six Metrotech Center.

†Associate Professor, Mechanical, Aerospace, and Manufacturing Engineering Department, Six Metrotech Center; votugen@rama.poly.edu. Senior Member AIAA.

‡Graduate Assistant, Mechanical, Aerospace, and Manufacturing Engineering Department, Six Metrotech Center.

I. Introduction

A LARGE volume of research has been carried out on jet flows in the past few decades, and a wealth of knowledge exists on the structure of planar symmetric[1–4] and round axisymmetric[5–11] turbulent jets with uniform exit conditions. Therefore, a firm understanding of the fundamental aspects of jets with symmetric and uniform initial property distributions exists. The very early investigations of these flows were limited to the distributions of mean velocity and pressure. Later, however, with the availability of hot-wire anemometry (and more recently laser Doppler velocimetry), time-resolved measurements became possible in turbulent jets. This led to a better understanding of the turbulent structure and mixing in both plane and axisymmetric jets. Information is available on the spreading and centerline property decay rates as well as the approach to self-preservation in such jets. The turbulent transport of heat and mass and its dependence on the organized large structures have also been investigated in plane symmetric and round axisymmetric jets by Browne and Antonia[12] and Zhu et al.,[13] respectively. The structure and mixing characteristics of these jets are dependent on the initial conditions at the exit plane, which include the boundary-layer thickness and type, turbulence level, and jet Reynolds number (in the moderate-Reynolds-number regime). These conditions also affect the length of the initial development zone (i.e., the region before the mean jet properties become self-preserving).

Research efforts have also been directed toward three-dimensional turbulent jets originating from noncircular orifices. These studies include jets from rectangular as well as elliptic orifices.[14–17] In the case of rectangular jets, the flow is characterized by the existence of three zones: the initial region, which includes the potential core, the two-dimensional jet-type region, and finally the axisymmetric jet-type region.[14] The two latter regions are identified by the corresponding velocity decay rates. The elliptic jet can be viewed as the intermediate case between the axisymmetric and the plane symmetric jet. In this geometry the flow development is strongly controlled by the dynamics of the initial vortex ring, and unusually high mixing rates can be achieved at some optimum aspect (major-to-minor axis) ratio.

Although the initial velocity profile can have an influence on the evolution of the turbulent jet, to the authors' best knowledge no systematic effort has been reported that quantifies such possible effects. For example, both the time-mean structure and the dynamics of the near field of a jet with a fully developed initial velocity profile is

markedly different than that with a uniform exit profile. The former jet lacks the potential core and the surrounding mixing layer, whose breakdown generates the highly energetic coherent turbulent structures that characterize the near field of the latter jet. These characteristics of the near-field flow structure are likely to cause a difference in the evolution of the two types of jets into a self-preserving state and in the asymptotic flow properties thereafter. There are practical applications where a jet emerges from a source with an asymmetric velocity distribution such as in jet ejectors and powered lift generators in advanced aircraft, as well as other types of duct exits downstream of sharp bends. These jets can have significantly different mean and turbulent velocity structures than their axisymmetric counterparts, especially in the initial development region before they have relaxed into symmetry.

In the present we investigate the effects of nonuniform initial-velocity profiles on the evolution of turbulent round jets. An experimental facility was built to generate turbulent jets with various types of initial velocity profiles. In this paper, two jets with nonuniform initial velocity profiles, one with an axisymmetric fully developed profile and the other with an asymmetric initial profile, are presented. Both jets had a Reynolds number of 2.4×10^4, based on the exit bulk velocity and the source diameter. The jets emerged into a still environment. A straight pipe was used to generate the jet with the axisymmetric fully developed exit profile. The source for the jet with the asymmetric initial velocity profile was a pipe with a 90-deg bend upstream of the exit, which provided the asymmetry on the horizontal plane. The mean exit properties of this second jet were symmetric on the vertical plane. Velocity measurements were made using hot-wire anemometry, from which the evolution of mean and turbulent velocity fields was determined. The effect of initial velocity distribution on jet growth rate, centerline velocity decay, and approach to self-preservation were determined. Turbulent kinematic properties of the jets such as turbulent viscosity and integral length scales have also been examined.

II. Experimental Facility and Instrumentation

The experimental setup used for the current work is shown in Fig. 1. High-pressure air was supplied through a set of regulators and a control valve into a 610-mm long cylindrical settling chamber with a diameter of 203 mm. At the downstream end the settling chamber was coupled with a steel pipe as seen in Fig. 1. The straight end of the pipe was connected to the settling chamber using an airtight rubber coupling, and the pipe protruded into the chamber approximately 50 mm to ensure an axisymmetric inlet into the pipe. Four different jet delivery pipes were used: two straight and two with a 90-deg bend at one end. The far-field measurements were performed

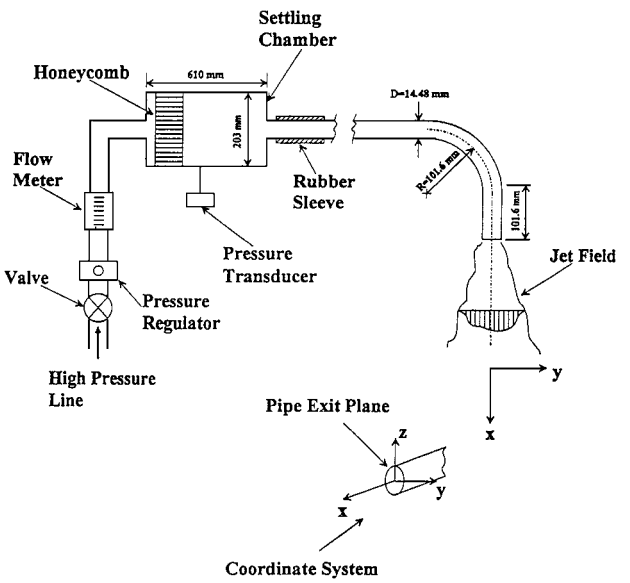

Fig. 1 Schematic of experimental setup.

with 14.5-mm diam pipes. In the near field up to $x/D < 15$, pipes with 25.4-mm diam were used to improve the spatial resolution of the measurements. The axisymmetric jet with the fully developed initial profile was produced by the straight pipes, whereas the axisymmetric jet was obtained using pipes with the 90-deg bend before the exit. For this case the pipe bends had a pipe diameter-to-mean radius of curvature ratio of $D/R = 0.142$. This resulted in a fixed Dean number of $De = 6400$ for the flow around the bend. Thus, the secondary motion through the bend and the level of skewness of mean streamwise velocity distribution at pipe exit was fixed for the asymmetric jet. (Figure 1 shows the asymmetric jet set up for the far-field study.)

The length-to-diameter ratio of the straight pipes was 80, thus allowing for a fully developed pipe flow at the exit of the axisymmetric jet. For the asymmetric jet the long straight section of the delivery pipes also had a length-to-diameter ratio of 80 producing a fully developed pipe flow condition upstream of the bend. Downstream, the curved pipes had 5-diameters long straight sections to allow for the flow to recover from the static pressure perturbation and the secondary flow cells introduced through the bend. Previous studies of turbulent flows through 90-deg (Ref. 18) and 180-deg (Refs. 19 and 20) bends at similar Dean numbers have shown that the circumferential gradients of the wall pressure and secondary flow cells essentially vanish within a distance of about 5 pipe diameters from the bend. Indeed, total, yaw, and wall static-pressure measurements we performed both immediately upstream of and at the pipe exit showed no circumferential pressure gradients or detectable secondary flow patterns.

The static pressure in the settling chamber was continuously monitored with a variable reluctance pressure transducer (Validyne Model DP7), and the settling chamber pressure was kept constant to within 1% to ensure a constant jet velocity. Before each experiment the rough adjustment of the flow rate was made using a flow meter placed upstream of the settling chamber. In fine adjustments two-dimensional surveys of the axial velocity at pipe exit were carried out using a pitot probe in conjunction with a personal computer equipped with an A/D board.

Both single and x-type sensors were used for the hot-wire measurements with TSI model 1050 constant temperature anemometers. The sensors were 1.2-mm-long tungsten wires with 11 μm diam. The anemometers were adjusted to provide frequency responses of approximately 13 kHz. The sensors were calibrated in a standard calibration air jet. Tangential cooling effects on the sensors were taken into account by calibrating each sensor at a range of yaw angles (up to ± 11 deg) and incorporating this in the measurements. A DAS-16F, 12-bit resolution A/D converter digitized instantaneous signals. Data acquisition was controlled by a computer equipped with a 80486 processor. Mean velocity and turbulence intensity were calculated from records of instantaneous velocity. The sampling rates and record lengths depended on the measurement location and varied from 100 Hz and 30 s (sampling rate and record length, respectively) in the jet near field to 60 Hz and 150 s for measurements in the region $x/D > 65$. The hot-wire and pitot probes were mounted on a traversing mechanism that allowed for continuous traverses along the horizontal y and vertical z directions. This two-axis traversing mechanism was mounted on an adjustable traverse rail that was aligned normal to the jet exit plane to allow motion along the jet axis x. The resolution on the y-z traversing mechanism was determined to be approximately 0.1 mm while the probe could be positioned in the x direction to within 0.5 mm. Under these conditions the measurement uncertainty is estimated to be 8, 10, 10, and 15% for U, u', v', and $u'v'$, respectively, in the near-field measurements. In the far-field these estimates are 4, 6, 6, and 11%, respectively.

III. Results and Discussion

In the following, we will refer to the jet with the fully developed, axisymmetric initial velocity profile as case I and the initially asymmetric jet as case II. The exit bulk velocity is determined by numerically integrating the two-dimensional distribution of the axial velocity obtained by using a pitot tube. The coordinate system for the jet flow is shown in Fig. 1. Here, x is the streamwise coordinate

along the jet axis while y and z are the cross-stream coordinates parallel and normal to the plane of pipe bend, respectively.

A. Near-Field Development

Velocity profiles measured at the exit of both jets along the z coordinate were found to be symmetric. The mean streamwise velocity profiles measured along the y axis in the development region of the jets are presented in Fig. 2. For case I the velocity profile at $x/D = 1$ is similar to that of a fully developed turbulent pipe flow except that inflection points have already formed near the edges of the jet. For case II the velocity near the jet exit exhibits an asymmetric streamwise velocity distribution with a maximum occurring away from the centerline and toward the outer edge of the jet (on the positive y half-plane). As the flow goes through the curved pipe upstream of the exit plane, the imbalance between the centrifugal force and the radial pressure gradient sets up a secondary motion. The fluid near the pipe axis moves outward while the fluid near the top and bottom walls moves inward.[21] This results in the distortion of the axial momentum distribution with higher velocities occurring near the outer wall of the pipe. The strength of the secondary motion and hence the degree of velocity skewness (asymmetry) depend on the Dean number, which is $De = 6400$ in the present work. The asymmetry in case II leads to two additional inflection points as compared to case I at jet exit. These additional inflection points persist up to $x/D = 9$. However, because of the fully shearing exit mean velocity profiles, the early stage development of both jets is rapid approaching a nearly Gaussian velocity distribution by $x/D = 9$. The initial decay of maximum velocity for case II is more rapid than for case I. This disparity is particularly prominent between $x/D = 1$ and 3, although even at $x/D = 9$, the case II jet has spread somewhat wider with a smaller maximum velocity as compared to case I. The location of maximum velocity in case II shifts rapidly toward the jet center reaching the centerline by $x/D = 9$, where the jet exhibits a nearly axisymmetric mean velocity profile.

The corresponding turbulence intensity profiles of the two jets are shown in Figs. 3 and 4. Within each jet the streamwise u' and lateral v' turbulence intensity profiles at respective streamwise stations are nearly identical. On the other hand, the initial turbulence structure of the two jets differs significantly. The profiles for case I are symmetric throughout (to within measurement uncertainty), whereas the profiles for case II show asymmetry near the jet exit. This initial asymmetry diminishes as the profiles approach symmetry by $x/D = 9$. At this station the turbulence profiles of the two jets look similar both in shape and in level. A comparison of Figs. 3 and 4 with Fig. 2 reveals the close coupling between the mean velocity distribution and turbulence intensity. For both jets the turbulence intensity peaks at locations where the mean velocity gradient is a local maximum. At the jet exit case I has a pronounced turbulence intensity peak on each side corresponding to the maximum mean shear location. The jet of case II has an additional turbulence intensity peak near the centerline caused by the sharp gradient of the mean velocity in this region. Overall, case II has higher initial turbulence intensity levels (both u' and v'), although the disparity vanishes by $x/D = 9$, again indicative of the rapid development of both jets toward a fully developed self-preserving state.

The Reynolds shear-stress profiles for the two jets are presented in Fig. 5. For case I $u'v'$ profiles are antisymmetric about the jet axis throughout. As expected, the value of the Reynolds shear stress is zero on jet axis, giving credence to the current measurements of $u'v'$. For case II the $u'v'$ profiles are initially nonsymmetric about the x axis, although they develop into antisymmetry by $x/D = 9$. Closer to the jet exit, higher shear-stress magnitudes are observed on the outer side of the jet. Further, in this initial development region the shear stress is nonzero on jet axis. The on-axis values of the shear stress are negative, whereas the corresponding mean velocity gradient observed in Fig. 2 is positive. In fact, the Reynolds shear stress and the transverse gradients of U carry opposite signs throughout both jets. This confirms the concept of gradient diffusion of turbulent momentum

$$-\rho u'v' = \mu_t \frac{\partial U}{\partial y} \tag{1}$$

even immediately downstream of the jet exit plane. Figure 6 shows the distribution of the estimated turbulent viscosity μ_t for case I, which is calculated from the measured profiles. To obtain the velocity gradient for the calculations, the velocity data were first fit to a sixth-order polynomial. Although the turbulent viscosity μ_t is positive throughout the field, it varies significantly both in the axial and radial directions with a definite growth trend in the axial direction. These large variations in the magnitude of μ_t would render the use of gradient transport-based turbulence models quite difficult in the near field of the jet.

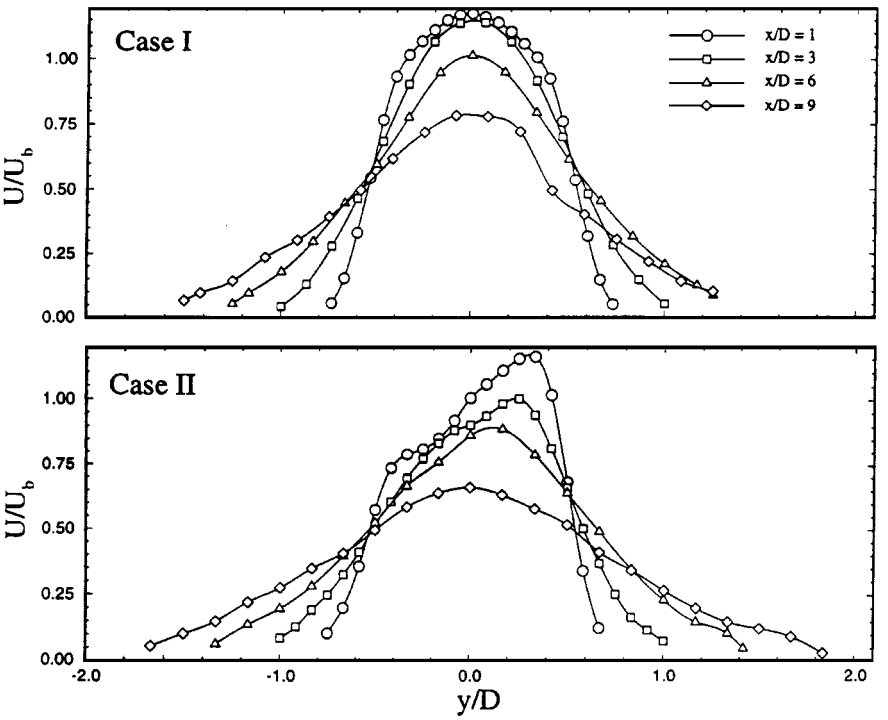

Fig. 2 Near-field profiles of mean streamwise velocity.

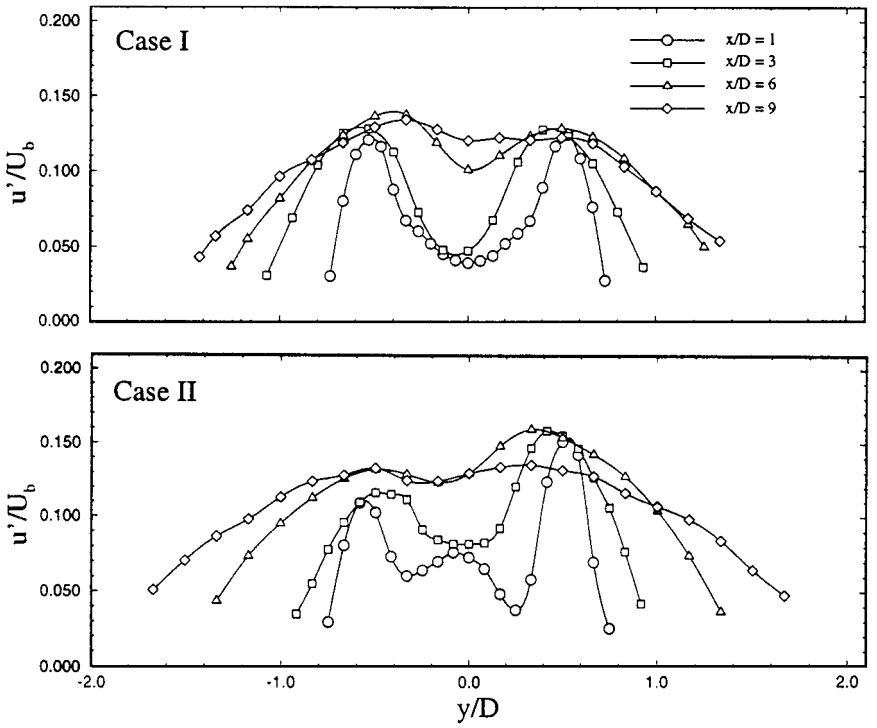

Fig. 3 Near-field profiles of streamwise turbulence intensity.

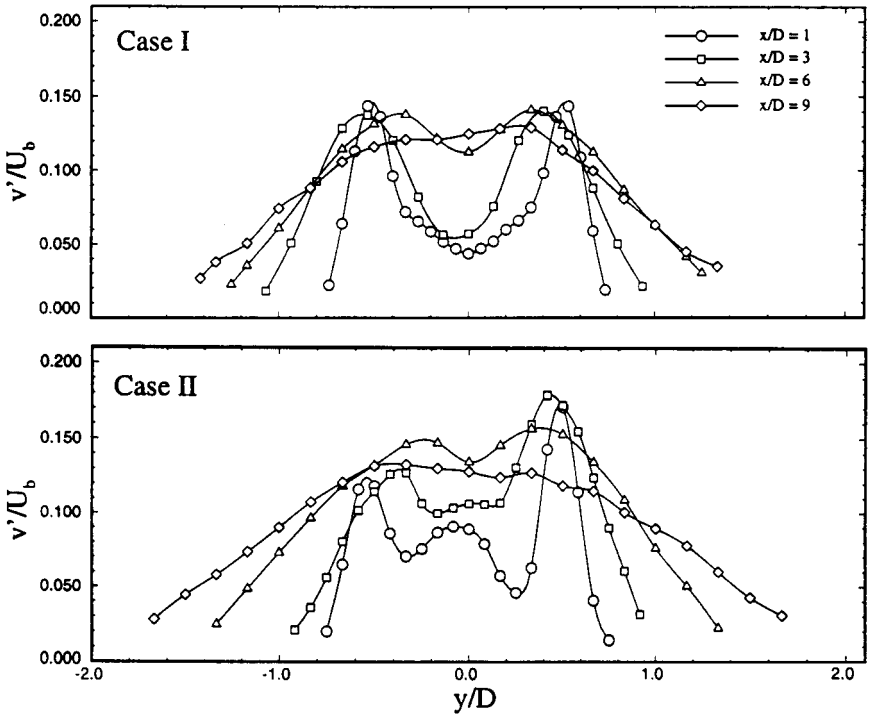

Fig. 4 Near-field profiles of transverse turbulence intensity.

B. Far-Field Trends

The far-field measurements covering the domain $15 \leq x/D \leq 80$ were carried out with jets exiting from 14.5-mm-diam pipes. The mean streamwise velocity profiles normalized by the local centerline (maximum) velocity are shown in Fig. 7. The lateral coordinate y is normalized by the jet half width b_u. All profiles for both jets collapse on a single curve showing that the mean velocity is self-preserving starting as early as $x/D = 15$. Furthermore, the Gaussian distribution

$$U/U_m = e^{-\ln 2(y/b_u)^2} \tag{2}$$

provides an excellent representation for the normalized velocity profiles for both jets. Clearly, no influence of the initial asymmetry is detected in the far-field velocity profiles of case II. The normalized streamwise velocity profiles along z coordinate are shown in Fig. 8. These profiles also indicate that case II is axisymmetric and both jets are fully developed for $x/D \geq 15$.

The turbulence intensity takes a longer axial distance to evolve into a fully developed state. As shown in Fig. 9, the streamwise turbulence intensity profiles do not become truly self-similar until about $x/D = 40$ for both jets. Beyond this axial location the collapse of u' profiles is well, and the two jets have nearly identical profiles. In

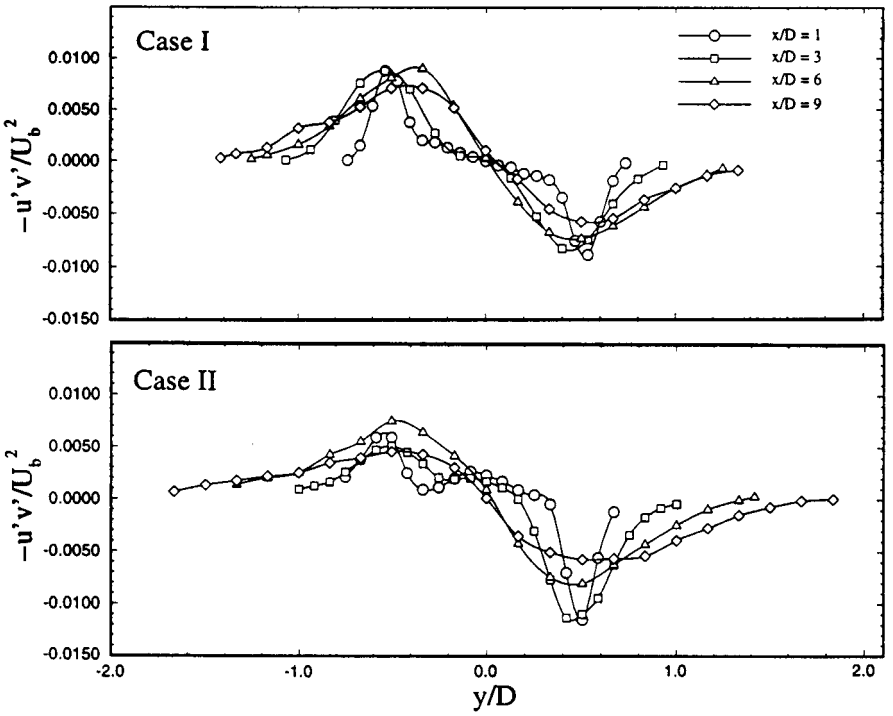

Fig. 5 Near-field profiles of Reynolds shear stress.

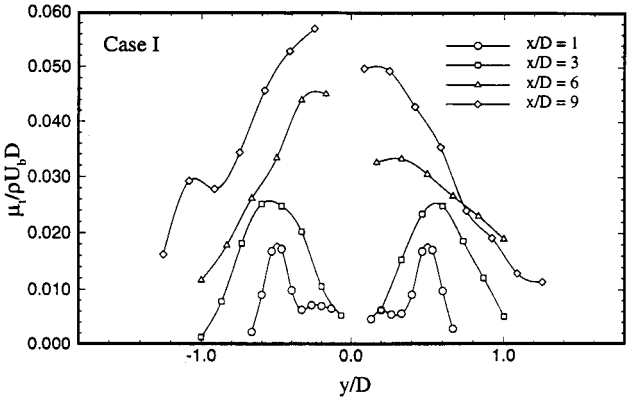

Fig. 6 Distribution of turbulent viscosity in the jet near field.

this self-preserving region the maximum turbulence intensity levels are around 0.25 for both jets. This value, on average, is smaller than those measured in round jets with uniform exit velocity profiles, which tend to be around 0.28–0.32 (see, for example, Refs. 6 and 22), with the exception of So et al.[11] who measured a value of 0.24 in a binary gas jet. The transverse turbulence intensity profiles of the two jets also look quite similar (Fig. 10). Interestingly, the transverse turbulence intensity seems to reach a self-similar state sooner than its streamwise counterpart as the profiles for v' are all grouped together with nearly the same shape throughout the domain. In addition, the v' profiles do not exhibit humps on the sides of the jet as in the case for u' profiles, and the levels of maximum turbulence intensity in the transverse direction are smaller that those along the streamwise direction. Clearly, the large structures in the flow responsible for the bulk of the turbulence intensity still have some directional preference in the far field, and the turbulence field cannot be assumed isotropic in any strict sense. The Reynolds shear-stress distributions along the y coordinate presented in Fig. 11 also show a reasonable degree of self-similarity. The small variations in these profiles are more likely caused by the relatively large levels of uncertainty inherent in the measurements of this quantity rather than a lack of self-preservation. In any case the Reynolds shear stress for case II is quite similar to that for case I both in trend and in level. The normalized maximum shear-stress level is about 0.014 for both of the present jets. This value also is slightly smaller than those obtained in axisymmetric jets with uniform initial velocity distributions that are in the range between 0.017 and 0.019 (see, for example, Refs. 6, 9, and 23).

The turbulent viscosity distributions shown in Fig. 12 are calculated using Eq. (1). The measured Reynolds shear-stress profiles are fit to a sixth-order polynomial, and the velocity gradients are calculated from the Gaussian distribution [Eq. (2)] to reduce the scatter in the calculated values. Because the uncertainty of the calculated μ_t grows very large for small y/b_u, data near the jet centerline are left out from the graphs while the centerline value is obtained by taking the limit of the function as $y/b_u \rightarrow \infty$. The trend of turbulent viscosity is similar for the two jets. Although the profiles do not seem to reach a self-preserving state within the flow domain investigated, the uncertainty in the calculated values perhaps has more to do with this than flow physics. All profiles fall within the uncertainty limits shown as dashed lines in Fig. 12. These uncertainty limits are obtained by calculating the propagations of random errors in measured $u'v'$. In determining μ_t, systematic errors may also occur, which can be caused, for example, by small angular deviations in the orientation of the x wire when measuring $u'v'$. This, indeed, seems to have happened in case I. As compared to case II, each side of the μ_t profile of case I seems to have rotated slightly in the clockwise direction. If this small rotation in case I is attributed to the slight misalignment of the hot-wire sensor in the measurement of the Reynolds stress, Fig. 12 indicates that the turbulent viscosity is relatively uniform in the central portion of both jets and becomes somewhat smaller near the edges. The average centerline values of the normalized turbulent viscosity are 0.021 and 0.018 for cases I and II, respectively.

The evolution of the centerline turbulence intensities u' and v' are presented in Fig. 13. For comparison, the u' results of So et al.[11] from a round jet with uniform exit profile are also presented. Initially, because of the nonzero centerline mean shear at its exit, case II has a higher turbulence intensity than case I. This disparity in centerline turbulence level vanishes by $x/D = 15$. Further downstream, the jet of case II has u' and v' behavior that is basically identical to that of case I. On the other hand, the growth of the centerline turbulence of these jets is slower than that with the top-hat initial velocity. In the latter the thin nozzle lip boundary layer at exit[13] evolves into an

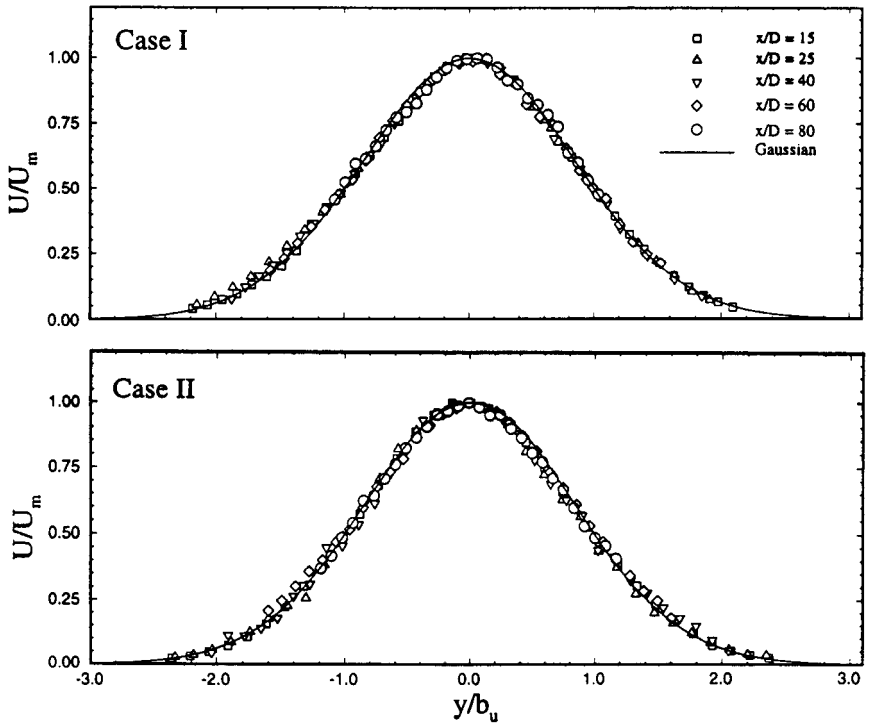

Fig. 7 Profiles of mean streamwise velocity along y.

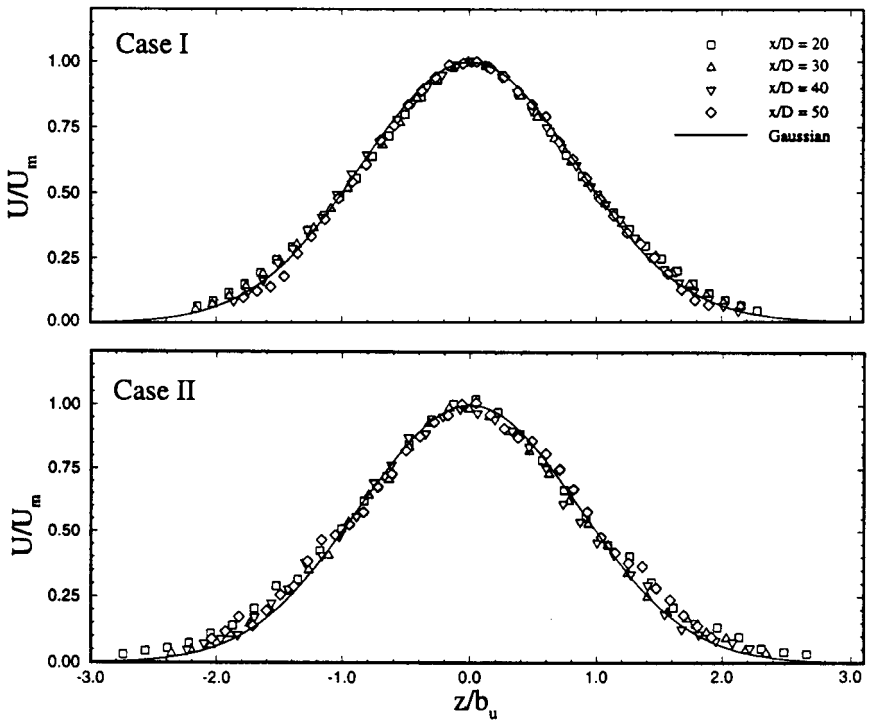

Fig. 8 Profiles of mean streamwise velocity along z.

unstable annular mixing layer whose breakdown generates highly energetic large turbulent structures, which, in turn, allow the rapid development of turbulence intensities in the near field. The centerline turbulence maximizes shortly downstream of the potential cone, where the annular mixing layer collapses onto itself, and it stays relatively constant thereafter. The present jets, which have fully shearing exit mean velocity profiles, lack such rapid generation and strong interaction of the dynamic turbulent structures. As a result, the approach to maximum turbulence is more gradual. Another feature observed in Fig. 13 is the disparity in the far-field evolution of u' and v'. Beyond $x/D = 25$, the centerline values of the streamwise and transverse turbulence intensity diverge reaching a constant ratio of $v'/u' \approx 0.77$ beyond $x/D = 65$. Thus, even on jet axis isotropy of turbulence cannot be assumed. The disparity between the axial and transverse turbulence intensity levels was observed also by other researchers who investigated both round and plane jets with uniform exit profiles,[6,9,24,25] and some attributed this manifestation of nonisotropy to the far-field remnants of large-scale coherent structures produced by the initial shear layer instabilities.[26] The present investigation shows that the initial shear layer instability has little to do with the lack of isotropy in the far field of the jet. The present jets are fully shearing at jet exit, and, hence, they do not lead to

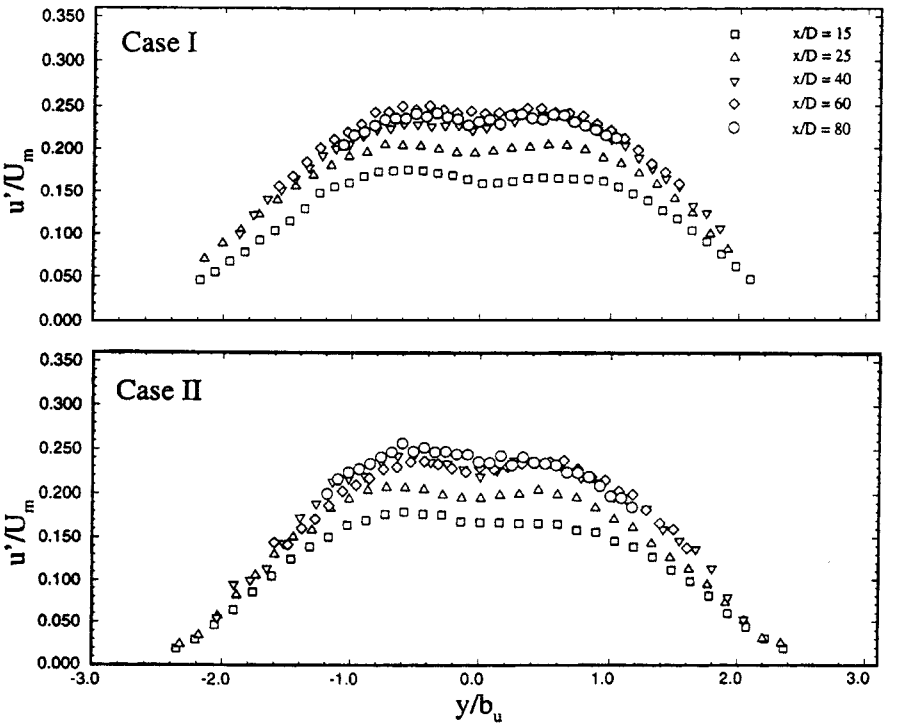

Fig. 9 Streamwise turbulence intensity profiles.

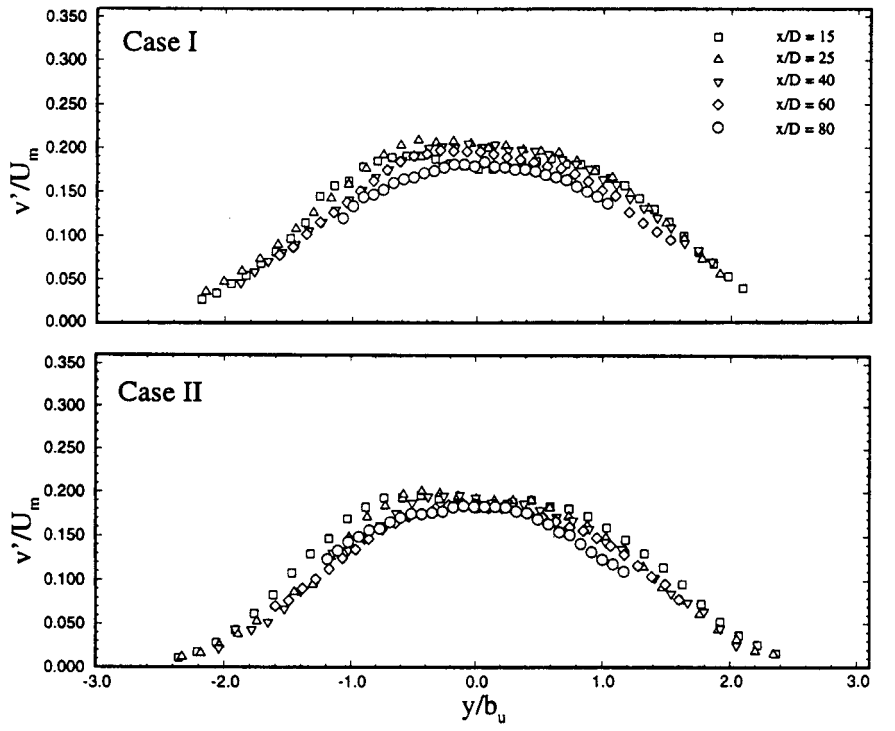

Fig. 10 Transverse turbulence intensity profiles.

quasi-periodic large-scale turbulent structures typical of the round and plane jets of past studies. The power spectra of fluctuating velocity in the near field of the present jets were studied extensively (not presented in this report), and this revealed no dominant frequencies. These results can be found in Ref. 27. Another conclusion that may be drawn from Fig. 13 is that if the fully developed state of a jet is based on turbulence kinematics, it is clear that the present jets do not evolve into such a state until about $x/D = 65$.

In the past several researchers have used the concept of effective jet diameter in order to account for the influence of initial mass and momentum distributions on jet evolution.[28–31] This approach was particularly effective in collapsing centerline decay data of binary gas jets when the axial distance was normalized by this new diameter.[32] The effective diameter is that of a hypothetical jet that has the same initial mass and momentum flux of the actual jet, but with a uniform initial property distribution and a density equivalent to that of the ambient.[33] For the present air-to-air jets an effective jet diameter, using the preceding concept, takes the form

$$D_E = \frac{2\int_A U_e \, dA}{\sqrt{\pi \int_A U_e^2 \, dA}} \tag{3}$$

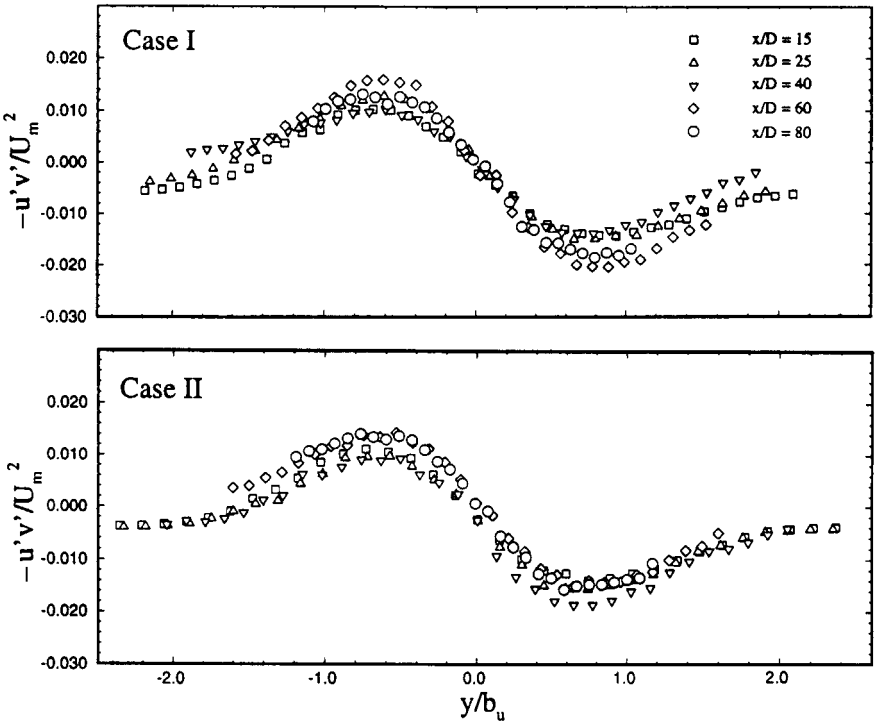

Fig. 11 Reynolds shear-stress profiles.

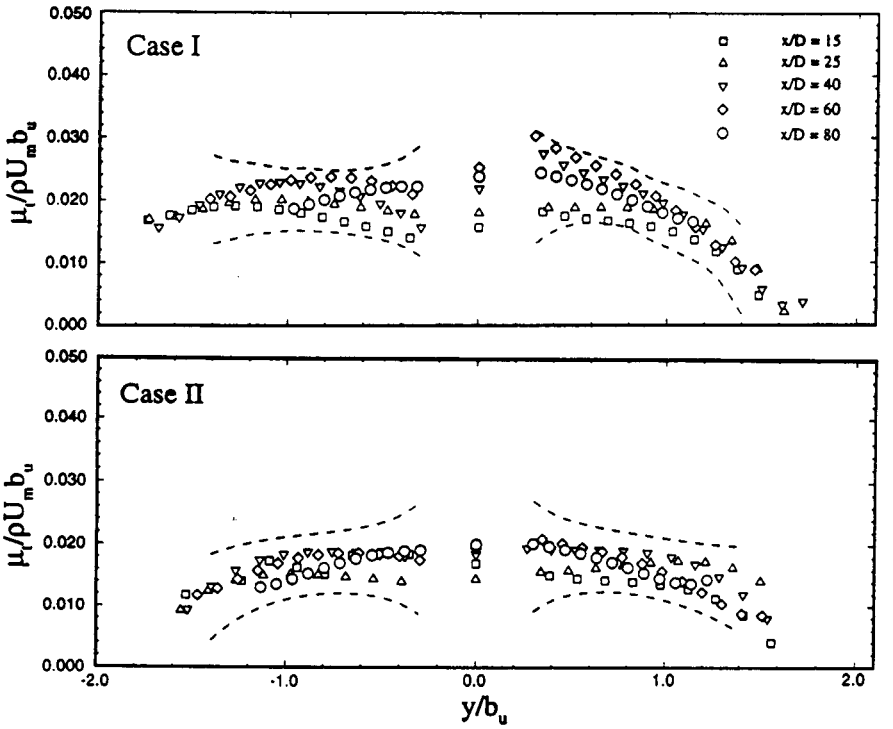

Fig. 12 Turbulent viscosity profiles.

However, the initial velocity distributions of the present jets are quite full, and the effective diameters calculated from Eq. (3) yield values that are within 1.5% of the actual pipe diameter. Therefore, the actual pipe diameter is used to normalize the axial distance in the graphs describing the jet growth and centerline velocity decay.

The decay of centerline mean velocity is presented in Fig. 14. The inverse of mean velocity can be expressed well by the linear expression

$$U_b/U_m = a(x/D) + a_e \tag{4}$$

for both jets. To obtain a meaningful comparison of the centerline velocity decay of jets with nonuniform velocity distributions, the local maximum velocity should be normalized by a bulk velocity derived from the initial momentum flux rather than the initial mass flux:

$$U_{b,1} = \frac{2}{\sqrt{\pi}D}\sqrt{\int_A U_e^2\,\mathrm{d}A} \tag{5}$$

Here $U_{b,1}$ is the initial velocity of a hypothetical jet that has the same initial diameter and momentum flux as the actual jet but with a uniform exit velocity distribution. Again, because the initial velocity profiles of the present jets are quite full, the calculated $U_{b,1}$

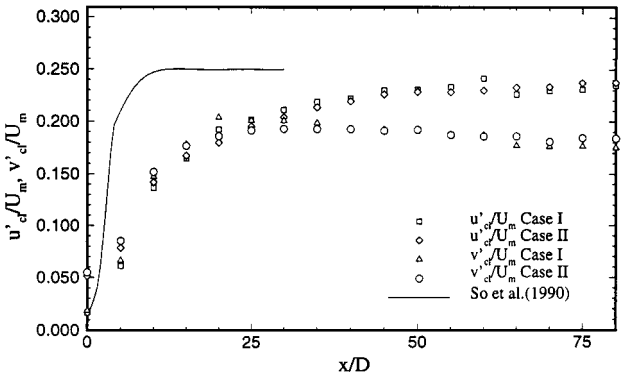

Fig. 13 Evolution of centerline turbulence intensity.

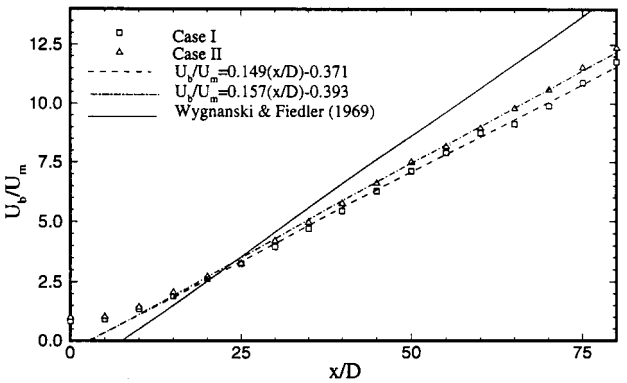

Fig. 14 Axial distribution of centerline mean velocity.

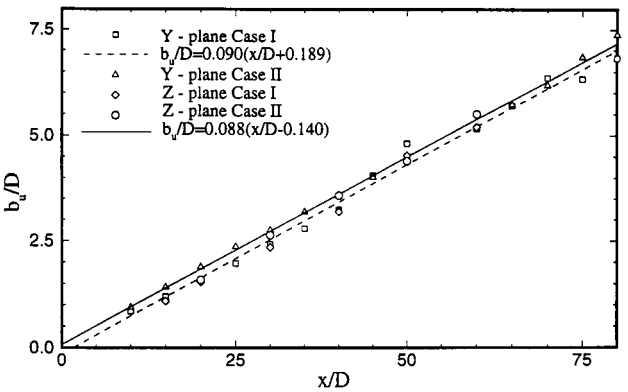

Fig. 15 Jet half-width growth.

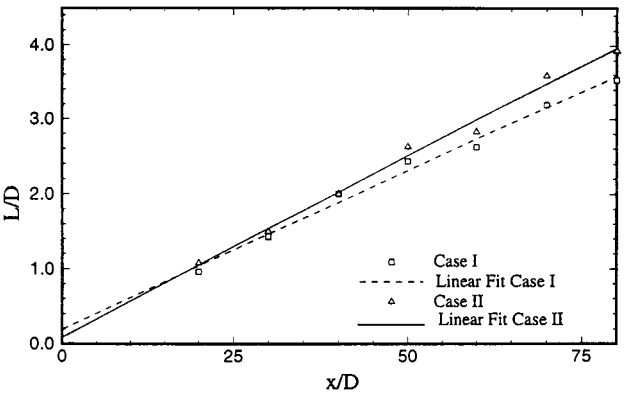

Fig. 16 Axial distribution of integral length scale.

values are very close to the mass flux-based bulk velocity U_b (to within 1.5%). Therefore, U_b rather than $U_{b,1}$, was used to normalize the centerline velocity in Fig. 14. The linear fits for the present jets were obtained by applying the least-square method to the data in the region $x/D \geq 15$. The centerline decay rate of the asymmetric jet is slightly larger than that of the axisymmetric jet, although the variation in the slopes is only about 5%. Both jets evolve into the linear decay mode at a relatively short distance downstream of the exit plane requiring only a small distance of adjustment. Thus, the linear fit of the data results in a virtual origin corresponding to a location of $x/D = 2.5$ for both case I and case II. This value is smaller than those typically obtained in jets with uniform initial velocity profiles showing that the present jets develop into a nearly self-preserving state at shorter distances from the exit. For example, the round jet of Wynganski and Fiedler[6] has a virtual origin about seven nozzle diameters downstream of the exit (Fig. 14). These researchers report that their reciprocal velocity curve did not become linear until about $x/D = 50$. Hence, the straight line representing their results in Fig. 14 is for $x/D > 50$. Linear fits of the present jets using data limited to $x/D \geq 30$ and 50 resulted in slope values that were within 5% of the those obtained using data in the range $x/D \geq 15$. The faster evolution of the present jets toward their asymptotic decay modes is caused by the lack of a potential core. However, the far-field centerline decay rates of the present jets are smaller than that of Ref. 6, which has a slope of ≈ 0.2. The weaker mixing rates characterizing the present jets can be attributed to the lack of highly energetic coherent structures that are produced in the initial development region of a jet with a top-hat initial velocity profile and a thin nozzle lip boundary layer. In those jets the initially thin, low-turbulence annular mixing layer develops instabilities and subsequently breaks down into vortical structures with kinetic energies (initially) of the order of the mean flow in the layer. The present jets have fully shearing initial velocity profiles that essentially prevent them from developing such high-energy structures. The shear layer is the full width of the jet with a higher level of turbulence. Therefore, they have significantly smaller average gradients and a much more efficient dispersion mechanism against instability development.

The growth rate based on the jet half width b_u is shown in Fig. 15. As shown in the figure, the average jet growth rate is based on the velocity profiles obtained on both the x plane and the z plane. As one would have expected from the centerline decay trends, the two jets have nearly identical growth rates. The growth of the jets is linear and is well represented by the following equation:

$$b_u/D = d(x/D) + d_e \tag{6}$$

The virtual origin (d_e) associated with the jet growth is small, once again, confirming the rapid development of the present jets into a nearly self-preserving state. In fully developed jets conservation of momentum provides a relationship between the rates of centerline velocity decay and jet growth. For nonbuoyant, uniform density round jets with Gaussian velocity distributions [Eq. (2)] and negligible virtual origins, the relationship is given by

$$a = (2/\ln 2)^{\frac{1}{2}} d \tag{7}$$

This linear relationship is confirmed in the present study, which yields $a/d = 1.67$ and 1.74 for cases I and II, respectively.

The integral length scale of turbulence was obtained from the autocorrelation functions measured at the jet centerline. The autocorrelations were transformed to two point spatial-correlation functions (separated in the streamwise direction) using the centerline mean velocity and thus invoking Taylor's hypothesis of frozen turbulence. The distribution of the integral length scale for the two jets are presented in Fig. 16. The integral length scale grows linearly with axial distance. The linear fit for each jet is obtained by using the least-square method. Although the figure indicates that case II has slightly larger integral length-scale values, this deviation between the two data sets is within measurement uncertainty. A comparison of Fig. 16 with Fig. 15 indicates that the integral length scale is roughly one half of b_u.

The jet momentum and mass flux values are shown in Figs. 17 and 18, respectively. These are calculated from the mean velocity

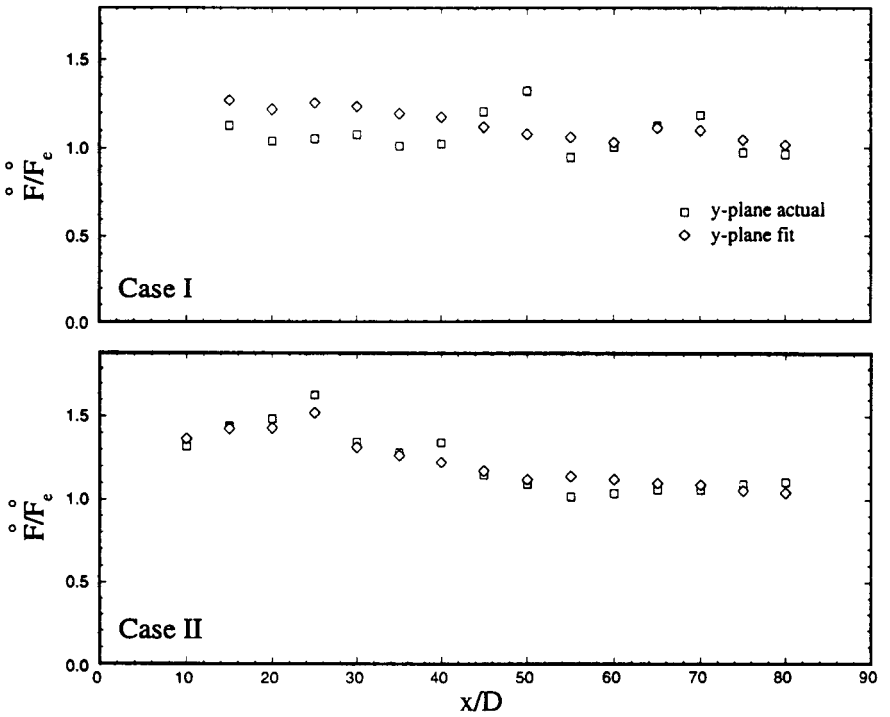

Fig. 17 Jet momentum flux.

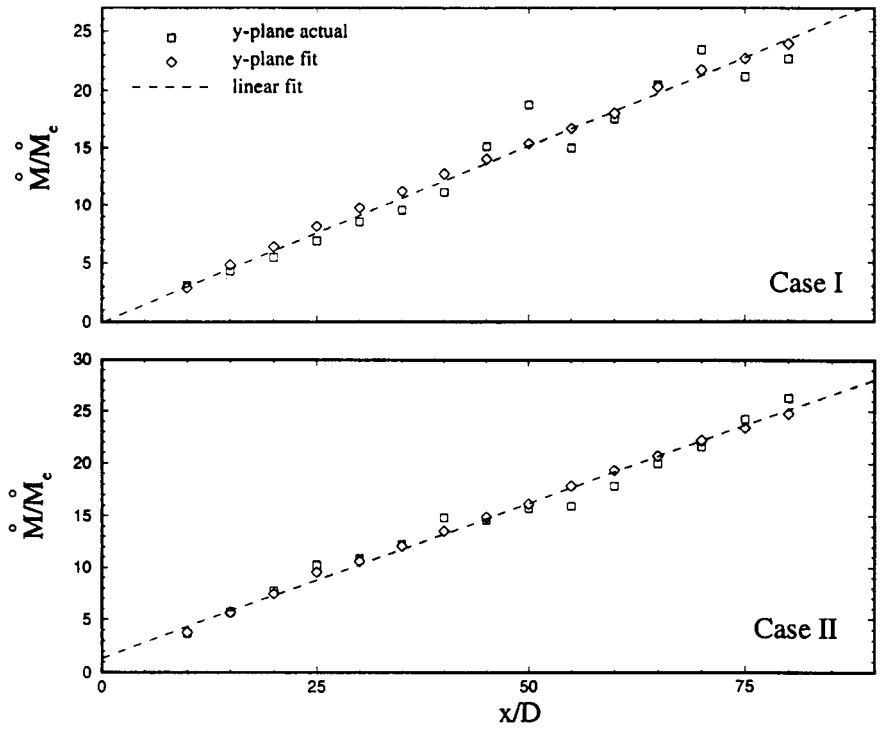

Fig. 18 Jet mass flux.

profiles on the y plane and using both the actual velocity data and the Gaussian fit of Eq. (2). In the absence of any global pressure or buoyancy effects, the jet momentum should be conserved throughout as $\dot{F}/\dot{F}_e = 1$. Figure 17 shows that the momentum flux is constant in the jet far field, whereas some deviations are observed for $x/D < 50$. Curiously, the normalized momentum flux reaches a peak value of 1.5 around $x/D = 25$ in case II. Figure 18 shows that the jet entrainment rate is linear and equal for both jets. Once again, the asymptotic rate for mass entrainment is attained very early in the jets ($x/D \approx 10$), and the entrainment-based virtual origin is nearly zero for both jets.

IV. Conclusions

The recovery of the jet in case II from the initial velocity asymmetry is rapid, and the flow becomes axisymmetric by an axial distance of about $x/D = 9$. In the initial development region up to $x/D = 9$, case II has larger overall turbulence intensities and spreading rates than case I. However, beyond $x/D = 15$ the two jets present nearly identical behavior. Approach of present jets toward a fully developed state, with self-similar mean-velocity profiles and linear centerline velocity decay rates, is faster than their counterparts with uniform initial profiles. This is attributed to the fully shearing initial-velocity profiles and the lack of a potential core in the present jets.

However, the lack of the potential core and the surrounding mixing layer (which subsequently breaks down to generate high turbulent energies and organized large structures) leads to slower centerline mixing and overall growth rates in the far field of the present jets. Correspondingly, the centerline turbulence intensities of the present jets are smaller than those of the already studied jets with top-hat initial velocity profiles. The present study demonstrates that jets with fully shearing initial mean-velocity profiles tend to have smaller far-field mixing and growth rates than the traditional jet from a convergent nozzle. The study also shows that the far-field behavior of jets with nonuniform initial velocity profiles are far less sensitive to differences in initial turbulence intensity levels and velocity profile shapes. The near-field radial and axial variation of turbulent viscosity is large, which would render the use of gradient transport-based turbulence models difficult in this region. In the far field the turbulent viscosity is relatively uniform in the central portion of the jet up to about $y/b_u < 1.2$.

References

[1]Haskestad, G., "Hot-Wire Measurements in a Plane Turbulent Jet," *Journal of Applied Mechanics*, Vol. 32, No. 4, 1965, pp. 721–734.

[2]Bradbury, L. J. S., "The Structure of a Self-Preserving Turbulent Plane Jet," *Journal of Fluid Mechanics*, Vol. 23, Pt. 1, Sept. 1965, pp. 31–64.

[3]Gutmark, E., and Wygnanski, I., "The Planar Turbulent Jet," *Journal of Fluid Mechanics*, Vol. 73, Pt. 3, Feb. 1976, pp. 465–495.

[4]Namer, I., and Otugen, M. V., "Velocity Measurements in a Plane Turbulent Air-Jet at Moderate Reynolds Numbers," *Experiments in Fluids*, Vol. 6, No. 4, 1988, pp. 387–399.

[5]Pai, S. I., "Axially Symmetric Jet Mixing of a Compressible Fluid," *Quarterly of Applied Mathematics*, Vol. 10, No. 2, 1953, pp. 141–148.

[6]Wygnanski, I., and Fiedler, H., "Some Measurements in the Self-Preserving Jet," *Journal of Fluid Mechanics*, Vol. 38, Pt. 3, Sept. 1969, pp. 577–612.

[7]Lau, J. C., Morris, P. J., and Fisher, M. J., "Measurements in a Subsonic and Supersonic Free Jets Using Laser Velocimeter," *Journal of Fluid Mechanics*, Vol. 93, Pt. 1, July 1979, pp. 1–27.

[8]Dimotakis, P. E., Miake-Lye, R. C., and Papantoniou, D. A., "Structure and Dynamics of Round Turbulent Jets," *Physics of Fluids*, Vol. 26, No. 11, 1983, pp. 3185–3192.

[9]Komori, S., and Ueda, H., "The Large Scale Coherent Structure in the Intermittent Region of the Self-Preserving Round Free Jet," *Journal of Fluid Mechanics*, Vol. 152, March 1985, pp. 337–359.

[10]Dahm, W. A., and Dimotakis, P. E., "Measurements of Entrainment and Mixing in Turbulent Jets," *AIAA Journal*, Vol. 25, No. 9, 1987, p. 1216.

[11]So, R. M. C., Zhu, J. Y., Otugen, M. V., and Hwang, B. C., "Some Measurements in a Binary Gas Jet," *Experiments in Fluids*, Vol. 9, No. 5, 1990, pp. 273–284.

[12]Browne, L. W. B., and Antonia, R. A., "Measurements of Turbulent Prandtl Number in a Plane Jet," *Journal of Heat Transfer*, Vol. 105, No. 3, 1983, pp. 663–665.

[13]Zhu, J. Y., So, R. M. C., and Otugen, M. V., "Mass Transfer in a Binary Gas Jet," *AIAA Journal*, Vol. 27, No. 8, 1989, pp. 1132–1134.

[14]Sforza, P. M., Stieger, M. H., and Trentacoste, N., "Studies on Three-Dimensional Viscous Jets," *AIAA Journal*, Vol. 4, No. 5, 1966, pp. 800–806.

[15]Trentacoste, N., and Sforza, P. M., "Further Experimental Results for Three-Dimensional Free Jets," *AIAA Journal*, Vol. 5, No. 5, 1967, pp. 885–891.

[16]Krothapalli, A., Baganoff, D., and Karamcheti, K., "On the Mixing of a Rectangular Jet," *Journal of Fluid Mechanics*, Vol. 107, June 1981, pp. 201–220.

[17]Hussain, F., and Husain, H. S., "Elliptic Jets: Part 1," *Journal of Fluid Mechanics*, Vol. 208, Nov. 1989, pp. 257–320.

[18]Enayet, M. M., Gibson, M. M., Taylor, A. M. K. P., and Yianneskis, M., "Laser-Doppler Measurements of Laminar and Turbulent Flow in a Pipe Bend," *International Journal of Heat and Fluid Flow*, Vol. 3, No. 4, 1982, pp. 213–220.

[19]Azzola, J., Humphrey, J. A. C., Iacovides, H., and Launder, B. E., "Developing Turbulent Flow in a U-Bend of Circular Cross-Section: Measurement and Computation," *Journal of Fluids Engineering*, Vol. 108, June 1986, pp. 214–221.

[20]Anwer, M., and So, R. M. C., "Frequency of Sublayer Bursting in a Curved Bend," *Journal of Fluid Mechanics*, Vol. 210, Jan. 1990, pp. 415–435.

[21]Berger, S. A., Talbot, L., and Yao, L. S., "Flow in Curved Pipes," *Annual Review of Fluid Mechanics*, Vol. 15, 1983, pp. 461–485.

[22]Chevray, R., and Tutu, N. K., "Intermittency and Preferential Transport of Heat in a Round Jet," *Journal of Fluid Mechanics*, Vol. 88, Pt. 1, Sept. 1978, pp. 133–160.

[23]Rodi, W., "A New Method of Analyzing Hot-Wire Signals in Highly Turbulent Flow and Its Evaluation in a Round Jet," *DISA Information Bulletin*, Vol. 17, 1975, pp. 9–18.

[24]Sreenivasan, K. R., Antonia, R. A., and Britz, K., "Local Isotropy and Large Structures in a Heated Turbulent Jet," *Journal of Fluid Mechanics*, Vol. 94, Pt. 4, Oct. 1979, pp. 745–775.

[25]Browne, L. W. B., Antonia, R. A., and Chambers, A. J., "The Interaction Region of a Turbulent Plane Jet," *Journal of Fluid Mechanics*, Vol. 149, Dec. 1984, pp. 355–373.

[26]List, E, J., "Turbulent Buoyant Jets and Plumes," *HMT The Science and Application of Heat and Mass Transfer*, edited by W. Rodi, Pergamon Press, Oxford, England, UK, 1992, pp. 16, 17.

[27]Ferdman, E., "An Experimental Investigation of the Initially Asymmetric Turbulent Jets," Master's Thesis, Dept. of Aeronautics and Astronautics, Polytechnic Univ., Brooklyn, NY, Jan. 1997.

[28]Thring, M. W., and Newby, M. P., "Combustion Length of Enclosed Turbulent Jet Flames," *Fourth (International) Symposium on Combustion*, Williams and Wilkins Co., Baltimore, MD, 1953, p. 789.

[29]Becher, H. A., Hottel, H. C., and Williams, G. C., "The Nozzle-Fluid Concentration Field of the Round, Turbulent, Free Jet," *Journal of Fluid Mechanics*, Vol. 30, Pt. 2, Nov. 1967, pp. 285–303.

[30]Avery, J. F., and Faeth, G. M., "Combustion of a Submerged Gaseous Oxidizer Jet in a Liquid Metal," *Fifteenth (International) Symposium on Combustion*, Combustion Inst., Pittsburgh, PA, 1975, p. 501.

[31]Dowling, D. R., and Dimotakis, P. E., "Similarity of the Concentration Field of Gas-Phase Turbulent Jets," *Journal of Fluid Mechanics*, Vol. 218, Sept. 1990, pp. 109–141.

[32]Pitts, W. M., "Effects of Global Density Ratio on the Centerline Mixing Behavior of Axisymmetric Turbulent Jets," *Experiments in Fluids*, Vol. 11, 1991, pp. 125–134.

[33]Papadopoulos, G., and Pitts, W. M., "Scaling of the Centerline Mixing Behavior in the Near Field of Axisymmetric Turbulent Jets," AIAA Paper 98-0695, Jan. 1998.